JOURNAL OF AGRICULTURAL AND FOOD CHEMISTRY

# Binding Model Construction of Antifungal 2-Aryl-4-chromanones Using CoMFA, CoMSIA, and QSAR Analyses

DENG-GUO WEI,† GUANG-FU YANG,*,† JIAN WAN,*,† AND CHANG-GUO ZHAN‡

Key Laboratory of Pesticide and Chemical Biology, Ministry of Education of China and College of Chemistry, Central China Normal University, Wuhan 430079, People's Republic of China, and Department of Pharmaceutical Sciences, College of Pharmacy, University of Kentucky, Lexington, Kentucky 40536

Flavonoids, generated by plants upon attack by a range of pathogens, are demonstrated to have a role in biotic and abiotic stress response phenomena in plants, and there is increasing evidence for the antibacterial, antifungal, and antiviral activities of these compounds. Using the bioisosterism strategy, a series of 2-aryl-4-chromanone derivatives based upon the structure of flavanones, a kind of flavonoid phytoalexins, were synthesized and tested for the antifungal activity against *Pyricularia grisea*, which have been reported in our previous papers. To further explore the comprehensive structure−activity relationship and construct the binding model for the antifungal compounds, two kinds of molecular field analysis techniques, comparative molecular field analysis (CoMFA) and comparative molecular similarity indices analysis (CoMSIA), were performed following a Hansch−Fujita QSAR study. Superimpositions were performed using three alignment rules, that is, centroid-based alignment, common substructure-based alignment, and field fit alignment, and statistically reliable models with good predictive power (CoMFA $r^2 = 0.952$, $q^2 = 0.727$; CoMSIA $r^2 = 0.965$, $q^2 = 0.751$) were achieved on the basis of the common substructure-based alignment. The combined results of CoMFA, CoMSIA, and former Hansch−Fujita QSAR analyses resulted in comprehensive understanding about the structure−activity relationships, which led to this construction of a plausible binding model of the title compounds.

**KEYWORDS: CoMFA; CoMSIA; Hansch−Fujita QSAR; 2-aryl-4-chromanones derivatives; binding model**

## INTRODUCTION

With the rapid progress in unraveling the biochemistry and molecular biology of defense pathways in plants, the secondary metabolites have been brought into sharp focus (*1*). Upon attack by a range of pathogens, plants activate a diverse array of defense pathways, which are mainly derived from the shikimic acid pathway that gives rise to the phenylpropanoid and flavonoid pathways. Flavonoids include diverse compounds, some of which are well-known phytoalexins and demonstrated to have a role in biotic and abiotic stress response phenomena in plants (*2*). There is increasing evidence for the antibacterial, antifungal, and antiviral activities of these compounds. Flavonoids have been suggested to be used as synthetic models to design new antifungals in recent decades (*3*−*6*).

Flavanones are well-known among the flavonoid phytoalexins. A drawback of using these phytoalexins as antifungal agent is that they are not easily translocated in the plant tissues due to the existence of polyhydroxyl groups in their molecular structures. Many studies have been performed on the structural modification and structure−activity relationships of flavanone derivatives (*3*, *4*, *7*−*12*). However, all of the modifications have been limited to the substituents on the aromatic moiety without any change to the skeletal framework, and most of the reported structure−activity relationships are of a qualitative nature. In addition, the mechanism of fungicidal action of phytoalexins has not yet been clearly established, and there is so far no report about the binding model of flavonoids with the receptor, which is crucial for the design of novel molecules. This paper aims to construct an initial binding model for flavonoids based on comprehensive understanding about the structure−activity relationships obtained from QSAR and 3D-QSAR analyses.

Toward this goal, as described in our previous papers, not only the variety of the substituent on the phenyl ring but also the effect of different heteroaryl rings on the antifungal activity was considered; a series of 2-aryl-4-chromanones were designed and synthesized in our laboratory via a bioisosterism strategy, and then a Hansch−Fujita QSAR study was performed on these synthesized compounds (*13*). Due to the limitations of every structure−activity approach, 3D-QSAR studies were performed in the present study using two kinds of molecular field analysis techniques: comparative molecular field analysis (CoMFA) and

* Corresponding authors (telephone: +86-27-6786-7706; fax +86-27-6786-2022; e-mail gfyang@mail.ccnu.edu.cn or jianwan@mail.ccnu.edu.cn).
† Central China Normal University.
‡ University of Kentucky.

10.1021/jf048313r CCC: $30.25 
Published on Web 02/08/2005

**Chart 1.** Frameworks of Molecular Structures **1**–**23** and **24**–**34** (See **Table 1** for the Definitions of the Substituents)

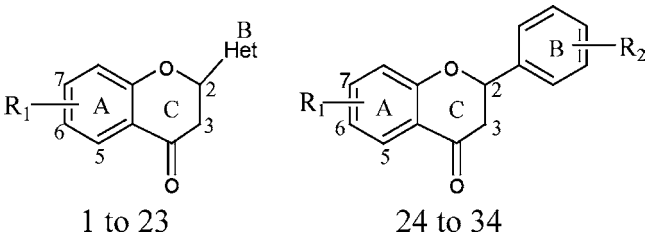


comparative molecular similarity indices analysis (CoMSIA). Both 3D-QSAR techniques compare a series of molecules in terms of molecular interaction fields; that is, they correlate field differences with differences in the dependent target property. For CoMFA, interaction fields are represented as steric and electrostatic interaction energies calculated using Lennard-Jones potential and Coulombic potential for a molecule in the data set at the intersections of a grid embedding that molecule (*14*). Another molecular interaction field is applied in CoMSIA (*15*), which uses Gaussian functions to describe the similarities of steric, electrostatic, hydrophobic, and hydrogen bond donor and acceptor properties (*16*). With different shapes of the Gaussian function, the similarity indices can be calculated at all grid points, both inside and outside the molecular surface.

## MATERIALS AND METHODS

**Data Sets for Analysis.** The title compounds (**1**−**34** in **Chart 1**) studied in this work were designed and synthesized in our laboratory to cover the potential range as widely as possible (*17*, *18*). All of the 34 compounds were purified by chromatography over silica gel, and their chemical structures were confirmed by $^1$HNMR spectra and mass spectroscopy as well as elemental analyses. The antifungal activity of the compounds against *Pyricularia grisea* was tested in vitro according to the modified method described previously (*18*). In the present study, the structures and biological activities of the training set (27 compounds) in the QSAR analyses and the test set (7 compounds) are listed in **Table 1**.

**Molecular Modeling and Alignment Rule.** All molecular modeling studies, CoMFA and CoMSIA, were performed using SYBYL 6.9 running on a Silicon Graphics Fuel workstation. Because of the highest potency, compound **2** was used in the systematic conformational search. First, all of the rotatable bonds in compound **2** were varied by using a step of 10°. Then, the lowest energy conformation identified in this conformational search was used as a template to build the other molecular structures. Each structure was energy-minimized using a conjugate gradient minimization algorithm with the Tripos force field until a gradient convergence of 0.001 kcal/(mol·Å) was achieved. Gasteiger−Hückel charges were calculated for all compounds.

Three different alignment rules were adopted in the present study. (1) Alignment I was centroid-based alignment. In this alignment, the centroids of phenyl ring and 2-aryl ring, the carbonyl carbon and the oxygen of the chromanone were used for RMS-fitting onto the corresponding atoms of the template structure. The atoms and the centroids used for the alignment were marked with an asterisk as shown in **Figure 1**. (2) Alignment II was common substructure-based alignment. It attempted to align molecules to the template molecule on the common backbone (4-chromanone), which is shown in **Figure 2** and used to determine the connectivity of the substructures to be matched. (3) Alignment III was a field fit alignment. This was carried out by the SYBYL QSAR rigid body field fit command within SYBYL. Field fit adjusted the geometry of the molecule such that its steric and electrostatic fields matched the fields of the template molecule. The results of the alignment of the molecules using these rules are shown in **Figure 3**.

**CoMFA and CoMSIA Descriptors.** CoMFA steric and electrostatic interaction fields were calculated at each lattice intersection on a regularly spaced grid of 2.0 Å. The grid pattern was generated automatically by the SYBYL/CoMFA routine and extended 4.0 Å units in X, Y, and Z directions beyond the dimensions of each molecule. An $sp^3$ carbon atom with a van der Waals radius of 1.52 Å and a +1.0

**Table 1.** Structures and Biological Activity of 2-Aryl-4-chromanones (See **Chart 1** for the Molecular Structures)

| | | | | $pI_{50}$ | | |
|---|---|---|---|---|---|---|
| compd | $R_1$ | het[a] | $R_2$ | obs | calcd[b] | calcd[c] |
| **1** | 7-$CH_3$ | I | | 5.90 | 5.77 | 5.82 |
| **2** | 7-$CH_3O$ | I | | 6.29 | 6.30 | 6.38 |
| **3** | H | I | | 5.14 | 5.16 | 5.22 |
| **4** | 6-$CH_3$ | I | | 5.89 | 5. 95 | 5.94 |
| **5** | 6-Cl | I | | 5.73 | 5.81 | 5.78 |
| **8** | H | II | | 4.66 | 4.63 | 4.64 |
| **9** | 7-$CH_3O$ | II | | 5.87 | 5.76 | 5.80 |
| **10** | 6-$CH_3$ | II | | 5.44 | 5.43 | 5.37 |
| **12** | 6-Cl | II | | 5.18 | 5.29 | 5.21 |
| **13** | 7-$CH_3O$ | III | | 6.04 | 6.12 | 6.03 |
| **14** | 6-Cl | III | | 5.84 | 5.78 | 5.78 |
| **15** | 6-$CH_3$ | III | | 5.84 | 5.91 | 5.93 |
| **16** | 6-Br | III | | 5.76 | 5.72 | 5.75 |
| **18** | H | IV | | 5.09 | 5.27 | 5.28 |
| **19** | 6-Br | IV | | 6.22 | 6.01 | 6.15 |
| **20** | 6-$CH_3$ | IV | | 6.13 | 6.08 | 6.01 |
| **21** | 6-Cl | IV | | 5.87 | 5.93 | 5.85 |
| **22** | 7-$CH_3$ | IV | | 6.01 | 6.02 | 6.03 |
| **24** | H | | 4-Cl | 5.73 | 5.77 | 5.68 |
| **25** | H | | 3-$NO_2$ | 5.85 | 5.68 | 5.72 |
| **26** | H | | 2-Cl | 5.36 | 5.38 | 5.39 |
| **27** | H | | 3-Cl | 5.38 | 5.37 | 5.33 |
| **28** | H | | 4-$OCH_3$ | 5.76 | 5.75 | 5.78 |
| **29** | H | | 4-$CH_3$ | 5.49 | 5.45 | 5.48 |
| **31** | H | | 4-F | 5.71 | 5.72 | 5.68 |
| **32** | H | | 2-Cl-6-F | 5.10 | 5.09 | 5.11 |
| **33** | 7-$CH_3$ | | 3-$NO_2$ | 6.23 | 6.36 | 6.36 |
| **6**[d] | 6-Br | I | | 5.83 | 5.89 | 6.08 |
| **7**[d] | 6-Br | II | | 5.40 | 5.38 | 5.50 |
| **11**[d] | 7-$CH_3$ | II | | 5.66 | 5.78 | 5.82 |
| **17**[d] | H | III | | 4.98 | 5.10 | 5.20 |
| **23**[d] | 7-$CH_3O$ | IV | | 6.24 | 6.40 | 6.44 |
| **30**[d] | H | | 2-F | 5.27 | 5.22 | 5.23 |
| **34**[d] | 6-Cl | | 3-$NO_2$ | 5.86 | 6.32 | 6.31 |

[a] I, 2-thienyl; II, 2-furanyl; III, 2-pyridinyl; IV, 3-pyridinyl. [b] Calculated using the CoMFA model based on the common substructure-based alignment. [c] Calculated using the CoMSIA model with the steric, electrostatic, and hydrophobic field based on the common substructure-based alignment. [d] These compounds were used as a test set and not included in the derivation of equations.

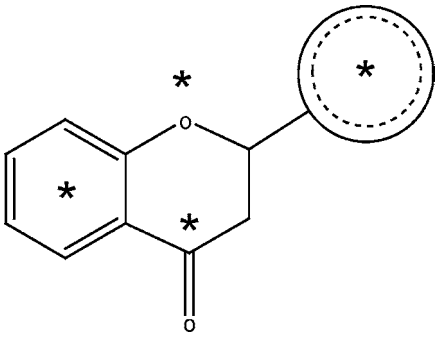


**Figure 1.** Centroid-based alignment.

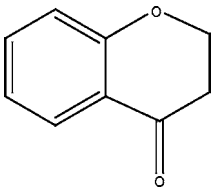


**Figure 2.** Common substructure alignment.

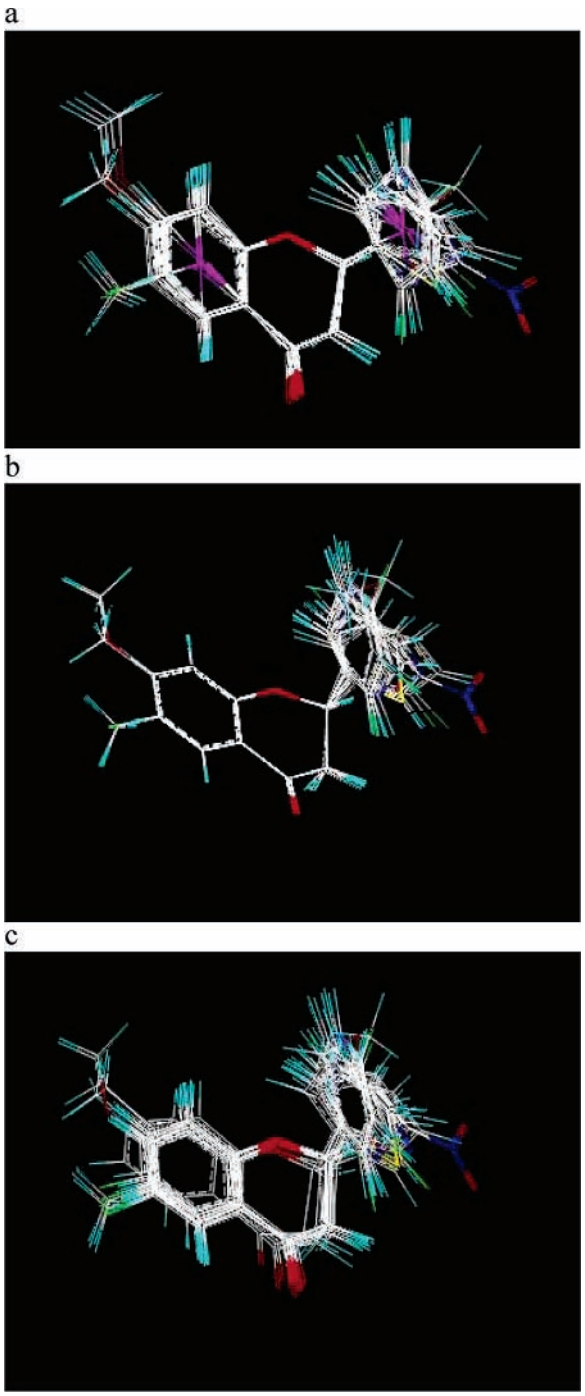


**Figure 3.** Superposition of compounds in the training and test sets: (**a**) centroid-based alignment; (**b**) common substructure-based alignment; (**c**) field fit alignment.

charge was used as the probe to calculate the steric (Lennard-Jones 6−12 potential) field energies and electrostatic (Coulombic potential) fields with a distance-dependent dielectric at each lattice point. Values of the steric and electrostatic fields were truncated at 30.0 kcal/mol. The CoMFA steric and electrostatic fields generated were scaled by the CoMFA-STD method in SYBYL. The electrostatic fields were ignored at the lattice points with maximal steric interactions.

CoMSIA calculates similarity indices at the intersections of a surrounding lattice. The similarity index $A_{F,k}$ for a molecule $j$ with atoms at the grid point $q$ is determined as follows

$$A^q_{F,k}(j) = \sum_i \omega_{\text{probe},k}\omega_{ik}\, e^{-\alpha r^2_{iq}}$$

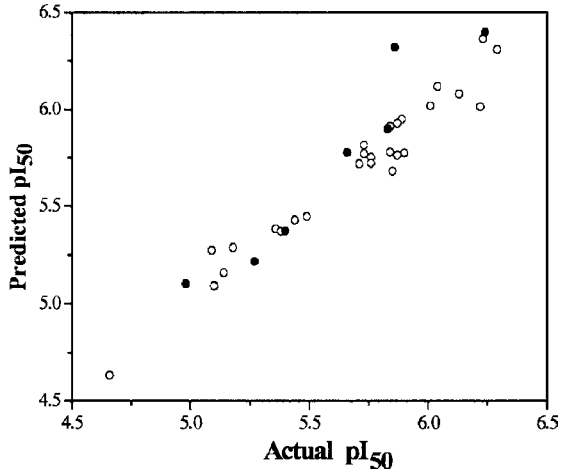


**Figure 4.** CoMFA predicted as experimental p$I_{50}$ values. Open circles represent predictions for the training set; solid circles represent predictions for the test set.

where $\omega_{ik}$ is the actual value of the physicochemical property $k$ of atom $i$; $\omega_{\text{probe},k}$ is the probe atom with a charge of +1, radius of 1 Å, hydrophobicity of +1, hydrogen bond donating of +1, and hydrogen bond accepting of +1; $r_{iq}$ is the mutual distance between the probe atom at grid point $q$ and the atom $i$ of the molecule. Due to the nonexistence of hydrogen donor in the title compounds, four physicochemical properties $k$ (steric, electrostatic, hydrophobic, and hydrogen bond acceptor) were evaluated, using a common probe atom with a radius of 1 Å, charge, hydrophobicity, and hydrogen bond accepting. A Gaussian-type distance dependence was considered between the grid point $q$ and each atom $i$ of the molecule. The value of the so-called attenuation factor α was set to 0.3. A lattice of 2 Å grid spacing was generated automatically.

A partial least-squares (PLS) approach (*20*−*22*), which is an extension of multiple regression analysis, was used to derive the 3D-QSAR, in which the CoMFA and CoMSIA descriptors were used as independent variables, and p$I_{50}$ values were used as dependent variables. The cross-validation with Leave-One-Out (LOO) option and the SAMPLS program (*23*), rather than column filtering, was carried out to obtain the optimal number of components to be used in the final analysis. After the optimal number of components was determined, a non-cross-validated analysis was performed without column filtering. The $q^2$ (cross-validated $r^2$), $s_{\text{press}}$ (cross-validated standard error of prediction), $r^2$ (non-cross-validated $r^2$), and $F$ values and standard error of estimate (SE) values were computed according to the definitions in SYBYL and are shown in **Table 2**. In **Table 2**, P$r^2$ = 0 means the probability of obtaining the observed $F$ ratio value by chance alone, if the target and the explanatory variables themselves are truly uncorrelated. If P$r^2$ = 0 is zero, then the results are not by chance and are significant.

In SYBYL/QSAR, the intensity of the cross-validation process is controlled by selecting the number of groups or the number of times the cross-validation step is to be carried out while predicting all rows (at each stage of model development). To perform an even more rigorous statistical test, several runs of cross-validation using five groups were done in which each target property value is predicted by a model based on about four-fifths or 80% of the available data. Also, to further obtain statistical confidence limits for the analysis, bootstrapping analysis (100 runs) was performed.

A common test to check the consistency of the models is to scramble the biological data and repeat the model derivation process, thus allowing detection of possible chance correlations. After our data set was randomized, very low or negative $q^2$ value were observed in all of the PLS analyses.

## RESULTS AND DISSCUSSION

The results of CoMFA and CoMSIA studies are summarized in **Table 2**. Among the three kinds of alignments, CoMFA

**Table 2.** Summary of Results from the CoMFA and CoMSIA Analyses

| | alignment I | | | | alignment II | | | | alignment III | | | |
|---|---|---|---|---|---|---|---|---|---|---|---|---|
| | CoMFA | CoMSIA[a] | CoMSIA[b] | CoMSIA[c] | CoMFA | CoMSIA[a] | CoMSIA[b] | CoMSIA[c] | CoMFA | CoMSIA[a] | CoMSIA[b] | CoMSIA[c] |
| $q^2$ | 0.680 | 0.716 | 0.761 | 0.754 | 0.727 | 0.738 | 0.751 | 0.756 | 0.662 | 0.630 | 0.760 | 0.731 |
| $s_{press}$ | 0.248 | 0.245 | 0.225 | 0.234 | 0.240 | 0.235 | 0.229 | 0.233 | 0.261 | 0.280 | 0.225 | 0.245 |
| $r^2$ | 0.908 | 0.921 | 0.968 | 0.973 | 0.952 | 0.923 | 0.965 | 0.970 | 0.948 | 0.920 | 0.961 | 0.960 |
| SE | 0.133 | 0.129 | 0.082 | 0.078 | 0.100 | 0.127 | 0.085 | 0.081 | 0.102 | 0.130 | 0.091 | 0.095 |
| compd | **4** | **6** | **6** | **7** | **6** | **6** | **6** | **7** | **5** | **6** | **6** | **7** |
| *F* value | 54.32 | 38.942 | 101.615 | 96.129 | 66.707 | 40.056 | 93.235 | 88.290 | 77.168 | 38.261 | 82.207 | 64.325 |
| $Pr^2 = 0$ | 0.000 | 0.000 | 0.000 | 0.000 | 0.000 | 0.000 | 0.000 | 0.000 | 0.000 | 0.000 | 0.000 | 0.000 |
| fraction | | | | | | | | | | | | |
| steric | 0.625 | 0.330 | 0.123 | 0.111 | 0.646 | 0.324 | 0.119 | 0.113 | 0.609 | 0.306 | 0.131 | 0.119 |
| electrostatic | 0.375 | 0.670 | 0.370 | 0.332 | 0.354 | 0.676 | 0.393 | 0.356 | 0.391 | 0.694 | 0.411 | 0.355 |
| hydrophobic | | | 0.507 | 0.456 | | | 0.489 | 0.432 | | | 0.457 | 0.389 |
| acceptor | | | | 0.102 | | | | 0.099 | | | | 0.136 |
| $r^2$ (bs)[d] | 0.926 | 0.939 | 0.968 | | 0.969 | 0.943 | 0.971 | | 0.972 | 0.941 | 0.965 | |
| SD[d] | 0.028 | 0.035 | 0.024 | | 0.019 | 0.034 | 0.020 | | 0.017 | 0.040 | 0.023 | |

[a] CoMSIA using the steric and electrostatic fields. [b] CoMSIA using the steric, electrostatic and hydrophobic fields. [c] CoMSIA using the steric, electrostatic, hydrophobic and hydrogen bond acceptor fields. [d] Results from 100 runs of bootstrapped analyses.

analysis based on the common substructure alignment resulted in models of the highest qualities ($q^2 = 0.727$, $r^2 = 0.952$, with six components). With respect to the CoMSIA analyses, three kinds of combinations were performed. Introducing hydrophobic field into the CoMSIA analyses using steric and electrostatic fields resulted in a great increase in the $q^2$ and $r^2$ values, which indicates that the hydrophobic property of the title compounds exhibits a significant effect on the biological activity. However, further introduction of the hydrogen bond acceptor fields into the CoMSIA did not improve the statistical significance as expressed by decreased or similar $q^2$ and $r^2$. Therefore, it may be concluded in this case that the hydrogen bond acceptor fields may bring the noise signals to the analyses, which can also be seen from the CoMSIA analyses result based on the second alignment separately with the steric, electrostatic, and hydrophobic fields, which gave $q^2$ values of 0.361, 0.487, and 0.546, respectively, whereas the $q^2$ value of CoMSIA analyses with the hydrogen bond acceptor fields is −0.064. As to the CoMSIA analyses using the steric, electrostatic, and hydrophobic fields, the analyses based on the common substructure alignment proved to be the best considering the predictive ability for the test set. Further test and analyses were performed on the CoMFA and the CoMSIA analyses based on the second alignment.

The LOO cross-validation method might lead to high $q^2$ values, which do not necessarily reflect a general predictability of the models. Therefore, cross-validation using five groups was performed. Because the randomness of the formation of the cross-validation groups may have a significant effect on the results, our cross-validation was performed 25 times for the analyses of CoMFA and CoMSIA using the steric, electrostatic, and hydrophobic fields based on the common substructure-based alignment. The results of cross-validation using five groups are reported in **Table 3**. Although the mean $q^2$ values were slightly lower as compared to the values obtained in the LOO method, both of the $q^2$ values are above 0.65. The results obtained suggest that there is a good internal consistency in the underlying data set.

The real test for the model predictability is to predict the activity of compounds that were not used in the model generation. Therefore, we used the test set consisting of seven compounds (compounds **6**, **7**, **11**, **17**, **23**, **30**, and **34**). The observed and calculated activity values for the training and test set molecules are given in **Table 1**, and the plots of the predicted versus the actual activity values for the training set and test set are shown in **Figures 4** and **5**, respectively. Both the CoMFA and CoMSIA models obtained from alignment II exhibited a good predictability on these compounds. The greatest advantage of CoMFA and CoMSIA is that the field effect on the target property can be viewed as 3D coefficient contour plots. The coefficient contour plots are helpful to identify important regions where any change in the steric, electrostatic, and hydrophobic fields may affect the biological activity, and they may also help to identify the possible interaction sites. In **Figures 6**−**10**, the isocontour diagrams of the field contributions ("stdev*coeff") of different properties obtained from the CoMFA and CoMSIA analyses (using the steric, electrostatic, and hydrophobic fields) based on alignment II are illustrated together with exemplary ligands.

**Table 3.** Results of Analyses with Cross-validation Using Five Groups

| | $q^2$ [a] | |
|---|---|---|
| | CoMFA | CoMSIA[b] |
| mean | 0.656 | 0.700 |
| high | 0.748 | 0.798 |
| low | 0.516 | 0.534 |

[a] Cross-validated $q^2$ using five groups with optimum number of components average of 25 runs. [b] Results of CoMSIA using the steric, electrostatic, and hydrophobic fields with alignment II.

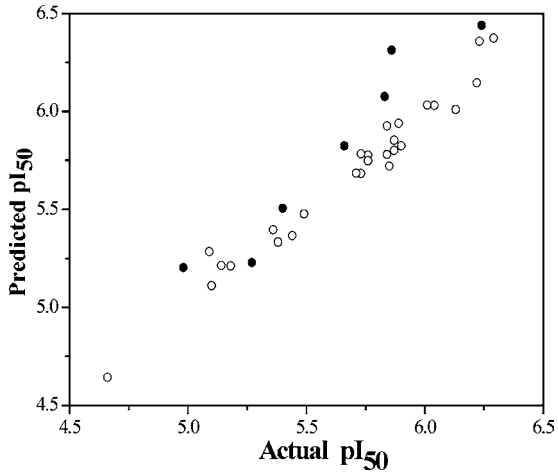


**Figure 5.** CoMSIA predicted versus experimental $pI_{50}$ values. Open circles represent predictions for the training set; solid circles represent predictions for the test set.

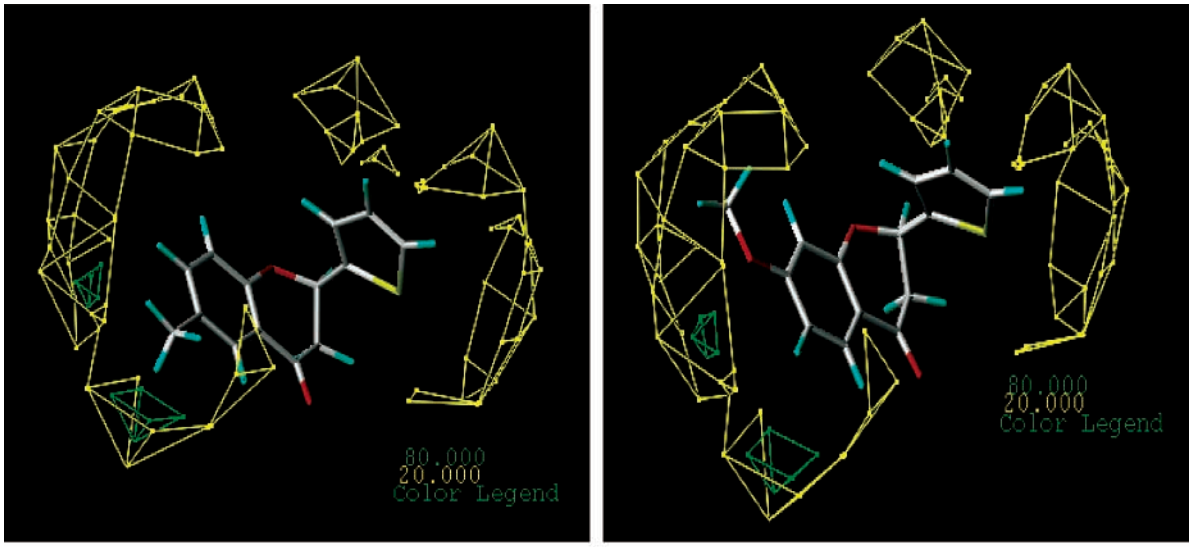


**Figure 6.** Steric maps from the CoMFA model using alignment II. Compound **4** (**a**) and compound **2** (**b**) are shown inside the field. Sterically favored areas (contribution level of 80%) are represented by green polyhedra. Sterically disfavored areas (contribution level of 20%) are represented by yellow polyhedra.

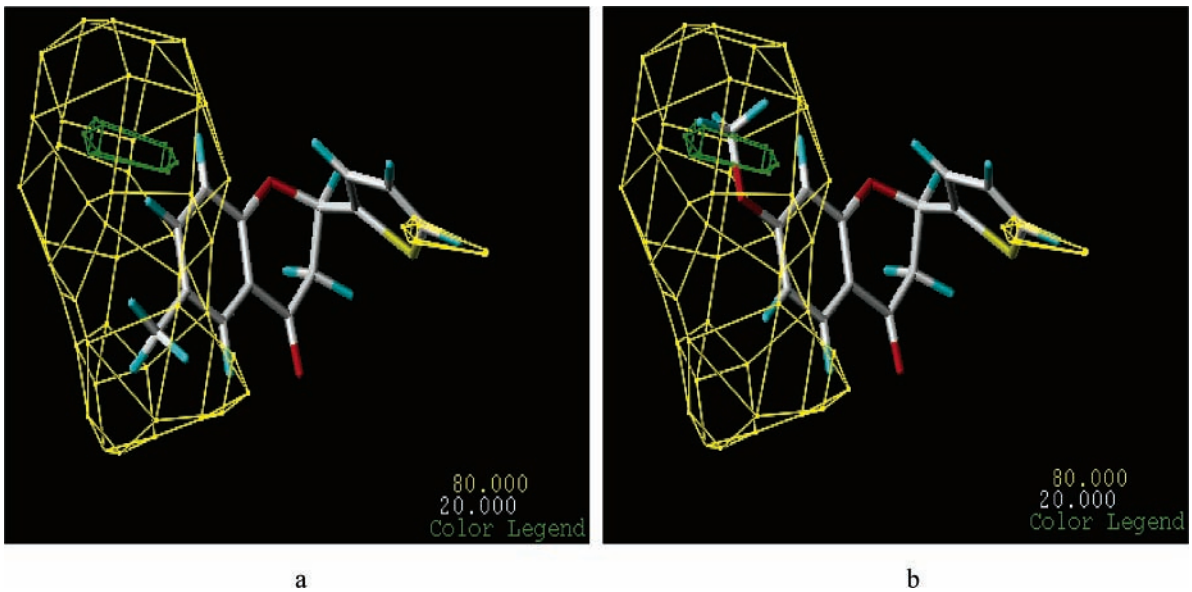


**Figure 7.** Steric maps from the CoMSIA model using the steric, electrostatic, and hydrophobic field with alignment II. Compound **4** (**a**) and compound **2** (**b**) are shown inside the field. Green contours (80% contribution) enclose areas where steric bulk will enhance affinity, and yellow contours (20% contribution) highlight areas that should be kept unoccupied.

The steric contribution contour maps of CoMFA and CoMSIA are plotted in **Figures 6** and **7**, respectively. The green and yellow polyhedra describe regions of space around the molecules where an increase in steric bulk enhances or diminishes the antifungal activity, respectively. As becomes immediately obvious, the CoMSIA approach provides more contiguous contour diagrams, which allows physicochemical properties relevant for binding to be mapped back onto the molecular structures. Furthermore, CoMSIA isocontour diagrams lie within regions occupied by the ligands, whereas CoMFA contours highlight those areas where the ligand would interact with a possible environment. Yet, the combined application of different approaches enables one to verify the convergence of the results, or the obtained conclusions can complement each other (*24*). From a small sterically favorable region and a very large sterically disfavored region surrounding the molecule revealed by both analyses, it can be concluded that the size of the binding site is limited. Green contours embedded in yellow contours indicate that there exists an optimal value for the steric effect. The CoMFA steric contour indicated obviously that the presence of the 6-substituent on the benzene ring is favorable and a comparison between compounds **3** and **4** shows that a change from a hydrogen to a methyl group at the 6-position increases the potency, which may be due to a suitable increase in the steric bulk of the group. However, in the CoMSIA contour, the green region is located around the 7-substituent of chromanone. The occupation of this area by a bulky group will have a positive effect on the antifungal activity as represented by compounds **2**, **9**, and **13**, which have higher antifungal activity than compounds **3**, **8**, and **17**, respectively. Compounds **2** and **4** are shown for reference in the steric contour plots. In this case, the combination of CoMFA and CoMSIA methods leads to a better

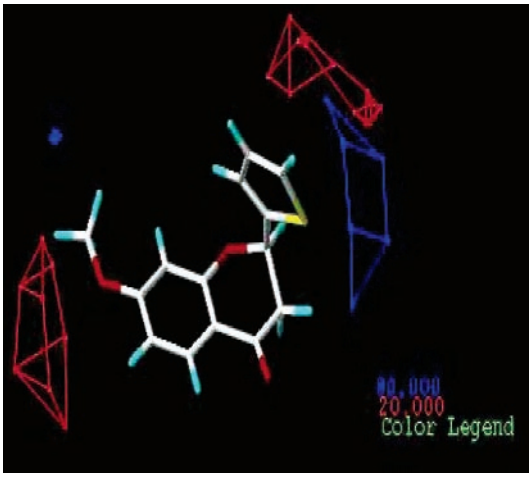


**Figure 8.** Electrostatic maps from the CoMFA model using the steric, electrostatic, and hydrophobic field with alignment II. Compound **2** is shown inside the field. Blue contours (80% contribution) encompass regions where an increase of positive charge will enhance affinity, whereas in red contoured areas (20% contribution) more negative charges are favorable for binding properties.

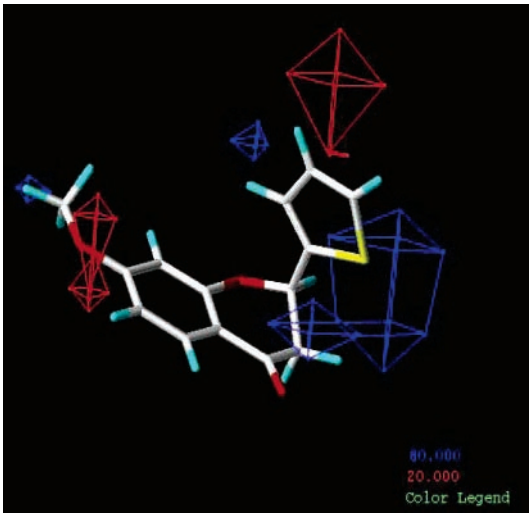


**Figure 9.** Electrostatic maps from the CoMSIA model using alignment II. Compound **2** is shown inside the field. Positive charge favored areas (contribution level of 80%) are represented by blue polyhedra. Negative charge favored areas (contribution level of 20%) are represented by red polyhedra.

interpretation for QSAR at the 3D level. However, it must be pointed out that the features derived from a comparative molecular field analyses depend on the structural variations inherently present in the selected data set. Selecting another structurally deviating data set might result in different results leading to alternative conclusions.

The electrostatic contour plots are shown in **Figures 8** and **9**. As opposed to the steric maps, CoMFA and CoMSIA analyses reveal essentially similar results here. The blue contour defines a region where increasing positive charge will result in increasing the activity, whereas the red contour defines a region of space where increasing electron density is favorable. A predominant feature of the electrostatic plot is the presence of a blue contour surrounding the B ring. It could be reasonably presumed that there is a significant electrostatic interaction between the B ring and the possible receptor, and it may be assumed that the faction of receptor around the blue region is

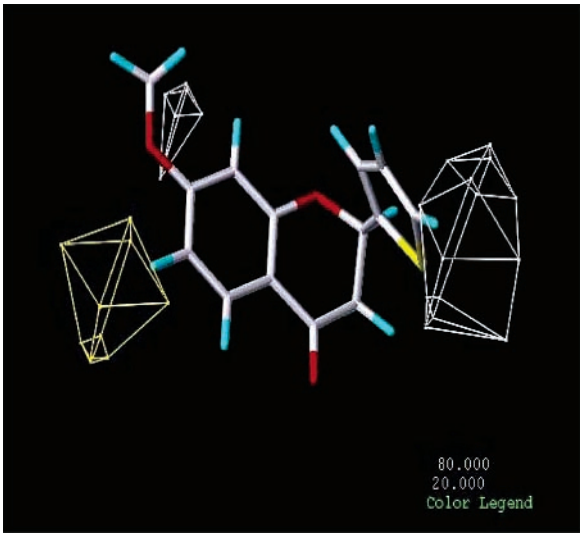


**Figure 10.** Hydrophobic field contour map of CoMSIA using the steric, electrostatic, and hydrophobic field with alignment II. Compound **2** is shown inside the field. Yellow regions (80%) indicate areas where hydrophobic groups increase activity, and white regions (20%) indicate areas where hydrophobic groups decrease activity.

electronegative. In both **Figures 8** and **9**, a red contour in the vicinity of the 6-substituents indicated that electronegative groups at this position could help to increase the activity. This is reflected in certain compounds, for example, **2**, **9**, and **13**, which possess electronegative substituents on the aromatic ring and have the high activity. Compound **2** was shown for reference in the electrostatic contour plots.

White and yellow contours of the currently reported CoMSIA model in **Figure 10** indicated the areas where hydrophilic and hydrophobic properties were preferred, respectively, and will be useful in selecting specific areas of the molecules to be utilized for adjusting the lipophilicity and hydrophilicity to improve antifungal activity. From the yellow area near the A ring just in the space where the green region appears in the steric contour of CoMFA, it could be reasonably assumed that there is a hydrophobic cavity in the receptor around the 6-substituent, producing hydrophobic interactions with the ligands. This can be seen from the activities of compounds **4**, **5**, and **14** that possess hydrophobic groups at the 6-substituent. A very distinct hydrophilic site existing near the B ring coincides with the positive charge favorable blue contour region, which suggests that there might be a $\pi-\pi$ stacking interaction between the B ring and the hydrophobic pocket of the possible receptor. Another hydrophilic site might exist near the 7-substituent. Compounds **2**, **9**, and **13** orient their $OCH_3$ groups in the white region, and their activity can be rationalized on the basis of their hydrophobic contour plot as shown in **Figure 10**.

Because flavonoids have been used as synthetic models to design new antifungal agents, a lot of studies have been carried out on the structure−activity relationships of them. Some studies indicated that flavonoid phytoalexins exert their toxicity by some membrane-associated phenomenon in most systems, which reveals the possible important effects of lipophilicity on their activity (*3*−*11*). The relative lipophilicities of flavonoid phytoalexins have been qualitatively compared and the relationship between the lipophilicity and antifungal activity has also been discussed qualitatively (*3*, *4*, *8*, *11*). Arnoldi et al. pointed out that within groups of compounds of similar structure, an increase in lipophilicity correlates positively with increased antifungal activity (*4*). Laks and Pruner studied the relationship between

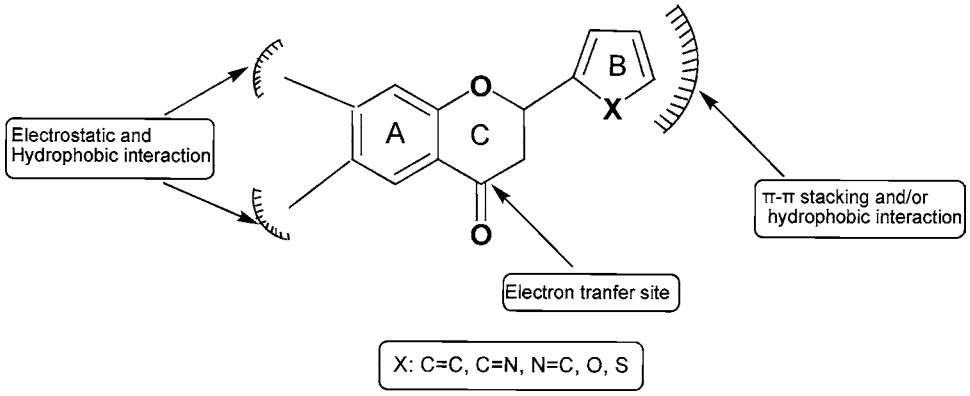


**Figure 11.** Schematic representation of possible binding model of antifungal 2-aryl-4-chromanone derivatives.

the lipophilicity and antifungal activity of two sets of semisynthetic flavonoid phytoalexin analogues, epicatechin-4-alkylsulfides and catechin dialkyl ketals, and found that the plots of the activity against *A. euteiches* and *F. solani* versus the lipophilic parameters ($R_M$) were parabolic (*11*). Our previously reported Hansch−Fujita QSAR was derived using descriptors such as CMR, $F^N_{C4}$, and ClogP. A parabolic model with ClogP was obtained in the study and revealed that there was an optimum ClogP value, that is, ClogP = 2.7, for the maximum antifungal activity for the data set. Therefore, to gain further insights into the role of hydrophobic interactions, hydrophobic fields of CoMSIA based on alignment II were computed and correlated separately with the antifungal activity, and the analyses gave a statistically significant model ($q^2 = 0.546$, $r^2 = 0.946$), which indicates that the hydrophobic effect looks to be a very important factor contributing to the biological activity. Besides, compared with the CoMSIA analyses using the steric and electrostatic fields, the $q^2$ and $r^2$ values of the CoMSIA with the combination of the hydrophobic, steric, and electrostatic fields in the correlation analyses were improved greatly. These results show the importance of hydrophobicity to the antifungal activity, and also the current hydrophobic field and steric field contour map of 3D-QSAR will be useful in selecting areas of molecules to be utilized for adjusting the lipophility to be a suitable value and avoiding any possible steric clashes for improved antifungal activity. The reported Hansch−Fujita QSAR also found some role of nucleophilic superlocalizability of the 4-position carbon atom ($F^N_{C4}$) for explaining the antifungal activity, and the positive coefficient of the $F^N_{C4}$ term indicated that the higher the approximate nucleophilic superdelocalizability of the carbon 4, the higher the activity, which suggests that there is an electron translocation between the carbonyl group and the receptor, and the greater the ability of the carbonyl group to accept electrons, the higher the activity. The CoMFA and CoMSIA analyses based on alignment II revealed electrostatic contributions of about 35.4 and 39.3%, respectively, which show the importance of the electrostatic field. Furthermore, 3D contour plots will be useful in identifying the positions where a more negative charge will increase or decrease the activity.

On the basis of the above studies, a plausible binding model of antifungal 2-aryl-4-chromanone derivatives with hypothetical receptor could be illustrated as shown in **Figure 11**. The carbonyl carbon may act as an electron-accepting site and interact with the electron translocation site of the receptor. There is an electrostatic and hydrophobic interaction between the 6,7-substituents and the receptor. The binding pockets for the 6-substituents and 7-substituents in the receptor are steric limited. In addition, the B ring may also act as an electrostatic and hydrophobic interaction site. The binding pockets might have strict geometrical orientation due to the rigid conformation of the flavonoids.

In conclusion, CoMFA and CoMSIA were performed following a Hansch−Fujita QSAR study to construct the binding model of antifungal 2-aryl-4-chromanone derivatives. For comparison, three different alignment rules including centroid-based alignment, common substructure-based alignment, and field fit alignment were used to obtain 3D-QSAR models. The 3D-QSAR models obtained from the common substructure-based alignment show better correlation with the antifungal activity and better predictability. The present work indicates that the combined analysis of the results of the CoMFA and CoMSIA analyses and further combination of the 3D-QSAR results with the Hansch−Fujita QSAR results enable us to obtain more comprehensive information about the structure−activity correlation. On the basis of the comprehensive understanding of the structure−activity relationships of the title compounds, a plausible binding model with the hypothetical receptor was constructed, which is expected to provide a helpful guideline for further designing novel potent antifungal agents. To our knowledge, this is the first report about the binding model of antifungal flavonoid phytoalexins.

## LITERATURE CITED

(1) Dixon, R. A.; Paiva, N. L. Stress-induced phenylpropanoid metabolism. *Plant Cell* **1995**, *7*, 1085−1097.

(2) Padmavati, M.; Reddy, Arjula R. Enhanced accumulation of flavonoids around the blast (*Pyricularia oryzae*) lesion site in rice (*Oryza sativa* L.), The Second International Electronic Conference on Synthetic Organic Chemistry (ECSOC-2). **1998**, Sept 1−30.

(3) Arnoldi, A.; Carughi, M.; Farina, G.; Merlini, L.; Parrino, M. G. Synthetic analogues of phytoalexins. Synthesis and antifungal activity of potential free-radical scavengers. *J. Agric. Food Chem.* **1989**, *37*, 508−512.

(4) Arnoldi, A.; Farina, G.; Galli, R.; Merlini, L.; Parrino, M. G. Analogues of phytoalexins. Synthesis of some 3-phenylcoumarins and their fungicidal activity. *J. Agric. Food Chem.* **1986**, *34*, 185−188.

(5) Weidenborner, M.; Jha, H. C. Antifungal activity of flavonoids and their mixtures against different fungi occurring on grain. *Pestic. Sci.* **1993**, *38*, 347−351.

(6) Weidenborner, M.; Jha, H. C. Antifungal spectrum of flavone and flavanone tested against 34 different fungi. *Mycol. Res.* **1997**, *101*, 733−736.

(7) Aida, Y.; Tamogami, S.; Kodama, O.; Tsukiboshi, T. Synthesis of 7-methoxyapigeninidin and its fungicidal activity against *Gloeocercospora. sorghi*. *Biosci., Biotechnol., Biochem.* **1996**, *60*, 1495−1496.

(8) Arnoldi, A.; Merlini, L. Lipophilicity-antifungal activity relationships for some isoflavonoid phytoalexins. *J. Agric. Food Chem.* **1990**, *38*, 834−838.

(9) Carter, G. A.; Chamberlain, K.; Wain, R. L. Investigations on fungicides. XX. The fungitoxicity of analogues of the phytoalexin 2-(2′-methoxy-4′-hydroxyphenyl)-6-methoxybenzofuran (Vignafuran). *Ann. Appl. Biol.* **1978**, *19*, 107−124.

(10) Adesanya, S. A.; O'Neill, M. J.; Roberts, M. F. Structure-related fungitoxicity of isoflavonoids. *Physiol. Mol. Plant Pathol.* **1986**, *29*, 95−103.

(11) Laks, P. E.; Pruner, M. S.; Flavonoid biocides: structure−activity relations of flavonoid phytoalexin analogues. *Phytochemistry.* **1989**, *28*, 87−91.

(12) Kodama, O.; Miyakawa, J.; Tadami, T.; Kiyosawa, S. Sakuranetin, a flavanone phytoalexin from ultraviolet-irradiated rice leaves. *Phytochemistry* **1992**, *31*, 3807−3809.

(13) Yang, G. F.; Jiang, X. H.; Yang, H. Z. Development of novel pesticides based on phytoalexins: part 2. Quantitative structure−activity relationships of 2-heteroaryl-4-chromanone derivatives. *Pest Manag. Sci.* **2002**, *58*, 1063−1067.

(14) Cramer, R. D., III; Patterson, D. E.; Bunce, J. D. Comparative molecular field analysis (CoMFA). 1. Effect of shape on binding of steroids to carrier proteins. *J. Am. Chem. Soc.* **1988**, *110*, 5959−5967.

(15) Klebe, G.; Abraham, U.; Mietzner, T. Molecular similarity indices in a comparative analysis (CoMSIA) of drug molecules to correlate and predict their biological activity. *J. Med. Chem.* **1994**, *37*, 4130−4146.

(16) Klebe, G.; Abraham, U. Comparative molecular similarity indices analysis (CoMSIA) to study hydrogen-bonding properties and to score combinatorial libraries. *J. Comput.-Aided Mol. Des.* **1999**, *13*, 1−10.

(17) Ding, Y.; Yang, G. F. Syntheses and fungicidal activity of B-cycle substituted flavanone derivatives. *Chinese J. Appl. Chem.* **2001**, *18*, 785−788.

(18) Yang, G. F.; Jiang, X. H.; Ding, Y.; Yang, H. Z. Development of pesticides based on phytoalexins. Part 1: Design and synthesis of flavanone analogues via bioisosterism substitution. *Chinese J. Chem.* **2001**, *19*, 423−428.

(19) Kearsley, S. K.; Smith, G. M. An alternative method for the alignment of molecular structures: maximizing electristatic and steric overlap. *Tetrahedron Comput. Methodol.* **1990**, *3*, 615−633.

(20) Wold, S.; Rhue, A.; Wold, H.; Dunn, W. J. I. The covariance problem in linear regression. The partial least squares (PLS) approach to generalized inverses. *SIAM J. Sci. Stat. Comput.* **1984**, *5*, 735−743.

(21) Wold, S.; Albano, C.; Dunn, W. J., III.; Edlund, U.; Esbensen, K.; Geladi, P.; Hellberg, S.; Johanson, E.; Lindberg, W.; Sjostrom, M. Multivariate data analysis in chemistry. *NATO ASI Ser., Ser. C* **1984**, *138*, 17−95.

(22) Clark, M.; Cramer, R. D., III. The probability of chance correlation using partial least squares (PLS). *Quant. Struct.-Act. Relat.* **1993**, *12*, 137−145.

(23) Bush, B. L.; Nachbar, R. B. Sample-distance partial least-squares PLS optimized for many variables, with application to CoMFA. *J. Comput.-Aided Mol. Des.* **1993**, *7*, 587−619.

(24) Boulamwini, J. K.; Assefa, H. CoMFA and CoMSIA 3D QSAR and docking studies on conformationally-restrained cinnamoyl HIV-1 integrase inhibitors: exploration of a binding mode at the active site. *J. Med. Chem.* **2002**, *45*, 841−852.

**Received for review October 11, 2004. Revised manuscript received November 18, 2004. Accepted November 18, 2004. The present work was supported by the National Key Project for Basic Research (2003CB114400, 2002CCA00500), National Natural Science Foundation of China (no. 20432010, 20172017, and 20203009), Program for Excellent Research Group of Hubei Province (no. 2004ABC002), and Program for New Century Excellent Talents in University of China.**

JF048313R